JPET Fast Forward. Published on November 13, 2017 as DOI: 10.1124/jpet.117.243865
This article has not been copyedited and formatted. The final version may differ from this version.

Restoration of rostral ventrolateral medulla cystathionine-γ lyase activity underlies moxonidine-evoked neuroprotection and sympathoinhibition in diabetic rats

Mohamed A. Fouda, Shaimaa S. El-Sayed and Abdel A. Abdel-Rahman

Department of Pharmacology, Brody School of Medicine,

East Carolina University, NC, U.S.A.

JPET Fast Forward. Published on November 13, 2017 as DOI: 10.1124/jpet.117.243865
This article has not been copyedited and formatted. The final version may differ from this version.

a) Running title: H_2S-dependent neuroprotection by moxonidine in diabetes

b) Corresponding author: Abdel A. Abdel-Rahman, Ph. D

Department of Pharmacology, Brody School of Medicine, East Carolina University, Greenville, NC 27834. Tel 252-744-3470; Fax: 252-744-3203

Email: abdelrahmana@ecu.edu

c) Number of text pages: 33

Number of tables: 0

Number of figures: 6

Number of references: 52

Word count:

Abstract: 227

Introduction: 416

Discussion: 1107

d) Abbreviations:

Diabetes mellitus (DM), cystathionine-γ lyase (CSE), Hydrogen sulfide (H_2S), Rostral ventrolateral medulla (RVLM), Reactive Oxygen Species (ROS), DL-propargylglycine (DLP), Hemeoxygenase-1 (HO-1).

e) Recommended section assignment: Endocrine and Diabetes

Abstract

We recently demonstrated a fundamental role for cystathionine-γ lyase (CSE)-derived hydrogen sulfide (H_2S) in the cardioprotective effect of the centrally acting drug moxonidine in diabetic rats. Whether a downregulated CSE/H_2S system in the rostral ventrolateral medulla (RVLM) underlies neuronal oxidative stress and sympathoexcitation in diabetes has not been investigated. Along with addressing this question, we tested the hypothesis that moxonidine prevents the diabetes-evoked neurochemical effects by restoring CSE/H_2S function within its major site of action, the RVLM. Ex-vivo studies were performed on RVLM tissues of streptozotocin (STZ; 55 mg/kg; i.p.)-diabetic rats treated daily for 3 weeks with moxonidine (2 or 6 mg/kg; gavage), H_2S donor NaHS (3.4 mg/kg; i.p), CSE inhibitor DL- propargylglycine (DLP; 37.5 mg/kg; i.p.), a combination of DLP with moxonidine or their vehicle. Moxonidine alleviated RVLM oxidative stress, neuronal injury, increased tyrosine hydroxylase immunoreactivity (sympathoexcitation) by restoring CSE expression/activity as well as HO-1 expression. A pivotal role for H_2S in moxonidine-evoked neuroprotection is supported by: (i) NaHS replicated the moxonidine-evoked neuroprotection, and the restoration of RVLM HO-1 expression in diabetic rats; (ii) DLP abolished moxonidine-evoked neuroprotection in diabetic rats, and caused RVLM neurotoxicity, reminiscent of a diabetes-evoked neuronal phenotype, in healthy rats. These findings suggest a novel role for RVLM CSE/H_2S/HO-1 in moxonidine evoked neuroprotection and sympathoinhibition, and as a therapeutic target for developing new drugs for alleviating diabetes-evoked RVLM neurotoxicity and cardiovascular anomalies.

Introduction

Diabetes mellitus (DM), a metabolic disorder, is associated with oxidative stress (Yan et al., 2014) as a result of ROS overproduction and reduction in antioxidant defense mechanisms (Ceretta et al., 2012; Fouda and Abdel-Rahman, 2017). The brain is more sensitive to oxidative stress, which affects gene expression and multiple cell functions (Giacco and Brownlee, 2010), due to its high oxygen consumption rate, plentiful lipid content and relatively limited antioxidant mechanisms (Abdel Moneim, 2015). While hydrogen sulfide (H_2S), similar to nitric oxide (NO) and hemeoxygenase (HO)-derived carbon monoxide (CO), protects against diabetes induced oxidative stress and cardiovascular complications (El-Sayed et al., 2016; van den Born et al., 2016), a mechanistic role for H_2S regulation in diabetes evoked neurotoxicity remains unknown.

Gasotransmitters modulate the interaction between the central cardiovascular regulation and metabolic disorders such as DM (Szczepanska-Sadowska et al., 2010), and affect many brain regions such as hippocampus, paraventricular nucleus, dorsal motor nucleus of the vagus, hypothalamus and rostral ventrolateral medulla (RVLM) (Biessels et al., 2002; Szczepanska-Sadowska et al., 2010). The RVLM regulates sympathetic tone and blood pressure (Pilowsky and Goodchild, 2002; Madden and Sved, 2003), and RVLM oxidative stress increases sympathetic activity (Konno et al., 2012). While high glucose-evoked neuronal oxidative stress (Bahniwal et al., 2017) might contribute to the neurotoxicity, sympathoexcitation and cardiovascular anomalies associated with diabetes, a definitive role for a dysfunctional cystathionine-γ lyase (CSE)/H_2S system in the RVLM of diabetic rats has not been investigated. Moreover, It should be noted that CO and H_2S synthesizing enzymes colocalize in discrete brain

JPET Fast Forward. Published on November 13, 2017 as DOI: 10.1124/jpet.117.243865
This article has not been copyedited and formatted. The final version may differ from this version.

areas (Ruginsk et al., 2015). Also, the H_2S-dependent induction of HO-1 in macrophages via extracellular signal-regulated kinase (ERK1/2) pathway (Oh et al., 2006) infers a similar crosstalk in other cell types. It remains unknown if a deficit in the H_2S/HO-1 signaling underlies diabetes induced neurotoxicity.

We have recently shown that moxonidine conferred cardioprotection by reversing the CSE/H_2S dysfunction in the heart of diabetic rats (El-Sayed et al., 2016). Notably, moxonidine, a well-known centrally acting imidazoline I_1 receptor agonist, improves cardiac function in hypertensive rats (Mukaddam-Daher et al., 2009). Also, H_2S modulates RVLM neuronal activity, which plays a vital role in hemodynamic control (Guo et al., 2011). Whether moxonidine protects RVLM neurons in diabetes and the mechanism of this neuroprotection have not been investigated.

The first objective of the current study was to ascertain a possible role for a deficit in CSE/H_2S in diabetes-evoked RVLM neurotoxicity and sympathoexcitation. Afterwards, we hypothesized that moxonidine mitigates the diabetes-induced RVLM neurotoxicity and sympathoexcitation by preserving neuronal CSE/H_2S/HO-1 signaling.

Materials and methods:

Animals:

Male Wistar rats (225–250 g, Charles River Laboratories, Raleigh, NC) were used and allowed free access to water and Purina chow (St. Louis, MO). Rats were retained on a balanced light-dark cycle and the temperature was kept at 22±1°C. All procedures were conducted in accordance with the Guide for the Care and Use of Laboratory Animals (2011) and approved by the institutional animal care and use committee.

Experimental groups:

The brains used in the present study (n=5/group) were obtained from treated and untreated diabetic, and control rats used in our recent study (El-Sayed et al., 2016). Briefly, male rats were fasted over night (16 hrs.), treated with a freshly prepared single dose of STZ (55 mg/kg, i.p.) in 0.1 M citrate buffer (pH 4) or the buffer (control), and drinking water was substituted with 5% dextrose for STZ-treated rats. Four weeks following diabetes induction (STZ injection), the rats were treated daily for 3 weeks with one of the following regimens or the vehicle (by the same route of administration): (i) H_2S donor, NaHS (3.4 mg/kg/day, i.p.); (ii) CSE inhibitor, DL-propargylglycine, DLP (37.5 mg/kg/day, i.p.); (iii) moxonidine (2 or 6 mg/kg/day, gavage); (iv) a combination of moxonidine (6 mg/kg) and DLP. At the end of the cardiovascular studies (El-Sayed et al., 2016), 7 weeks after STZ injection, the animals were euthanized by over-dose of pentobarbital, brains were collected, flash frozen in 2-methylbutane (Sigma-Aldrich, St Louis, MO) in dry ice, and stored at -80°C untill processed for the neurochemical studies detailed below.

Neurochemical Studies:

The RVLM was anatomically identified with the coordinates -12.6 to -11.8 mm relative to bregma (Ibrahim and Abdel-Rahman, 2015), and used for the neurochemical measurements, described below. For histochemical measurements, 3 coronal sections containing the RVLM (14 μm; approximately 0.05 mm) were cut at -24°C with a microtome cryostat (HM 505 E; Microm International GmbH, Walldorf, Germany). The remaining RVLM tissue was collected with a 0.75 mm punch instrument (Stoelting Co., Wood Dale, IL), homogenized with PBS (for ROS measurement; 50 mM, pH 7.4) or with lysis buffer (for western blot analysis).

Quantification of neurodegeneration (Fluorojade-C staining)

Modified protocols for immunofluorescence used in our previous studies (Wang and Abdel-Rahman, 2005) were used for staining degenerated neurons with a fluorescent Nissl counter stain (Yang et al., 2015). A fluorojade C staining kit was used in accordance with the manufacturer's instructions (Biosensis, TR-100-FJ, Thebarton, South Australia). Slides, containing the brain sections, were incubated in 0.06% potassium permanganate solution for 10 min followed by rinsing in distilled water for 2 min and then incubated in fluorojade C solution (1:25) for 30 min. The slides were then washed and mounted on coverslips with Vecta-shield mounting medium (Vector, Burlingame, CA, USA). A Zeiss LSM 510 confocal microscope (Carl Zeiss Inc., Thornwood, New York), and a blue (450–490 nm) excitation light was used for the visualization of stained neurons and image acquisition (Yang et al., 2015). For quantification, the fluorescence intensity was measured in the RVLM, using Zen Lite 2011 software, in brain sections from treatment and control groups (n=5 brains/group).

JPET Fast Forward. Published on November 13, 2017 as DOI: 10.1124/jpet.117.243865
This article has not been copyedited and formatted. The final version may differ from this version.

RVLM Caspase-3 expression

The immunohistochemistry technique described in our studies (Wang and Abdel-Rahman, 2002; Nassar et al., 2012) was used for measuring RVLM caspase-3 expression. Briefly, RVLM sections were post-fixed for 2 hrs. in 4% paraformaldehyde in tris-buffered saline, and subsequently incubated in 0.3% H_2O_2 for 30 min to block endogenous peroxidase. Sections were then incubated with anti-caspase-3 polyclonal antibody (1:1000; Abcam, Cambridge, USA) over night at 4°C using a modification of the avidin–biotin-complex method (ABC) kit (Vector Laboratories, Inc. Burlingame, CA). For validation, control sections incubated only with the primary or secondary antibody showed no positive staining (data not shown). Neuronal profile counts, denoting the total number of caspase-3 immunoreactive neurons, were used for quantification of caspase-3 expression in identical region (field=0.125 mm^2) of the RVLM of treated and control rats (n=5). Positive profiles exhibited dark granular brown staining indicative of a 3, 3-Diaminobenzidine (DAB) reaction product. The average per-field count of positive neuronal profiles was then determined and subsequently converted into the number of profiles per unit area (mm^2) for each rat brain (Marcus et al., 1998).

ROS measurement

Oxidative stress was measured using 2', 7'-dichlorofluorescein diacetate (DCFH-DA), a general detector of oxidative species (Rezq and Abdel-Rahman, 2016; Fouda and Abdel-Rahman, 2017). Briefly, a stock solution of DCFH-DA (20 mM, Molecular Probes, Grand Island, NY) was prepared in methanol and kept at -20°C protected from light. Punched RVLM tissues from treated and control groups were homogenized in PBS (50 mM, pH 7.4) and centrifuged at 14,000 rpm for 20 min at 4°C. Bio-Rad protein

assay was used to quantify the proteins in the supernatant. DCFH-DA stock solution was freshly diluted with PBS to prepare a150 μM working solution. The reaction was initiated by adding 10 μl of RVLM homogenate supernatant in a 96-well plate to give a final concentration of 25 μM DCFH-DA to produce fluorescent 2′,7′-Dichlorofluorescein (DCF) in the incubation medium at 37°C. Measuerment of fluorescence intensity started 30 min later using a microplate fluorescence reader set at excitation 485 nm/emission 530 nm. The standard curve of DCF was constructed and ROS level was determined as relative fluorescence units (RFU) of generated DCF (Rezq and Abdel-Rahman, 2016).

Dihydroethidium staining for superoxide detection

Following the recent recommendations of utilizing 2 or more different methods for ROS levels measurement (Griendling et al., 2016), frozen brain sections containing the RVLM from treated and control rats (n = 5) were incubated with 10 μM dihydroethidium (DHE) (Molecular Probes, Grand Island, NY) at 37°C in the presence of 5% CO_2 in a moist chamber for 30 min. The Assay was validated using positive and negative controls. A Zeiss LSM 510 microscope was utilized for image visualization. Image J Software (National Institutes of Health) was used for quantification and the changes in total fluorescence intensity, normalized to control, were calculated (Collin et al., 2007).

Western blot analysis

The detection and quantification of the expression of CSE, heme oxygenase-1 (HO-1) and tyrosine hydoxylase (TH) enzymes were followed as described in our previous studies (El-Sayed et al., 2016; Rezq and Abdel-Rahman, 2016; Fouda and Abdel-Rahman, 2017). Punched RVLM tissues were collected, as described above, and

homogenized with lysis buffer containing 20 mM TRIS, Ph 7.5, 150 mM NaCl, 1 mM EDTA, 1 mM EGTA, 1 % Triton x-100, 2.5 mM sodium pyrophosphate, 1 mM β-glycerophosphateand 1 µg/ml leuptin with protease inhibitor cocktail (Roche diagnostics, Indianapolis, IN). After homogenization and centrifugation, a Bio-Rad protein assay system (Bio-Rad laboratories, Hercules, CA) was used to quantify proteins in the supernatant. Twenty µg of each protein were applied per lane of 4-12 % SDS/PAGE gel (Invitrogen, Carlsbad, CA) and transfer was done using nitrocellulose membranes, then the proteins were revealed by immunoblotting using a 1:500 dilution of anti CSE, TH or HO-1 polyclonal antibodies along with 1:5000 dilution of anti-GAPDH (for CSE and TH) or anti-β-actin (for HO-1) (Abcam) at 4°C overnight. Afterwards, the membranes were washed, incubated for 60 min with mixture containing IRDye680-conjugated goat anti-mouse and IRDye800-conjugated goat anti-rabbit (1:15000; LI-COR Biosciences). The idetified proteins were visulaized using Odyssey Infrared Imager and analyzed with Odyssey application software version 5.2 (LI-COR Biosciences). Data represents mean values of integrated density ratio of CSE, HO-1 or TH normalized to the corresponding housekeeping protein, GAPDH or β-actin, and expressed as percent of nondiabetic control.

Measurement of RVLM H_2S synthesizing activity

The method described in our previous study (El-Sayed et al., 2016) was used. Punched RVLM tissues from different groups were homogenized in PBS (50 mM, pH 7.4), centrifuged and the protein, in the supernatant, was quantified using a Bio-Rad protein assay system. We added 100 µl sample (200 µg protein) to 900 µl of the reaction mixture (100 mM potassium phosphate buffer “pH 7.4”, 10 mM L-cysteine and

2 mM pyridoxal 5′-phosphate). Cryovial tubes (2 ml) containing 0.5 ml of 1% zinc acetate and a filter paper (1×1.5 cm) to increase the air-liquid contact, were used to trap the released H_2S gas. The bottles were flushed with nitrogen and sealed with parafilm double layers. We started the reaction by incubating the bottles in a shaking water bath (37°C) for 90 min. The reaction was stopped by addding 500 µl of 50% trichloroacetic acid; the bottles were sealed again and returned to the shaking water bath for another 60 min to ensure trapping of all generated H_2S. The contents were then transferred into Eppendorff tubes, and mixed with 134 µl each of N,N dimethyl p-phenylene diamine sulfate (20 mM) and ferric chloride (30 mM) followed with 20 min incubation at room temperature. Finally, the contents were transferred into 96 well plate and read at 650 nm in a microplate reader. We calculated H_2S concentrations using a calibration curve constructed with NaHS solution in 50 mM potassium phosphate buffer, pH 6.8 (0-320 µM NaHS equivalent to 0-96 µM H_2S). H_2S concentration was calculated as 30% of the NaHS concentration as reported (Velasco-Xolalpa et al., 2013; El-Sayed et al., 2016), and RVLM H_2S enzyme synthesizing activity was expressed as nmol/mg protein/min.

Drugs

The following drugs and chemicals were used in the present study. Moxonidine (American Custom Chemicals Corp., San Diego, CA), DL-propargylglycine (Chem-Impex International Inc., Wood Dale, IL), N, N dimethyl P-phenylenediamine sulfate (Acros Organics “Thermo Fischer Scientific”, Bridge water, NJ), acrylamide 40% (Fischer Scientific, Pittsburg, PA). All other chemicals were purchased from Sigma-Aldrich Company (St Louis, MO, USA).

Data analysis and statistics

Data are expressed as mean ± standard error of mean (SEM). Statistical analyses were conducted by one-way or repeated measures analysis of variance for multiple comparisons followed by Tukey's post hoc test and student's t-test using Prism 5.0 software (Graphpad software Inc., San Diego, CA); $P < 0.05$ was considered significant.

Results

Moxonidine mitigates STZ-induced RVLM neurodegeneration and oxidative stress

Fluorojade C staining, indicative of neuronal injury (Chaparro et al., 2013), was used to determine the number of RVLM damaged neurons. The RVLM of STZ-diabetic rats or DLP (CSE inhibitor)-treated non-diabetic rats exhibited approximately two-fold higher number of damaged neurons, compared to the non-diabetic (vehicle-treated) control group (Fig. 1). Moxonidine (dose-dependantly) or NaHS (H_2S donor) reduced ($P<0.05$) the number of RVLM damaged neurons in STZ-diabetic rats, and DLP abolished the neuroprotective effect of moxonidine (6 mg/kg) in STZ-treated rats (Fig. 1).

Similar to fluorojade findings, the number of RVLM caspase-3 immunoreactive neurons was higher ($P<0.05$) in STZ-diabetic, and in DLP-treated nondiabetic rats, compared to the nondiabetic control group (Fig. 2). Moxonidine (dose dependently) or NaHS (H_2S donor) reduced ($P<0.05$) the number of RVLM caspase-3 immunoreactive neurons in STZ-treated rats, and the neuroprotective effect of moxonidine (6 mg/kg) in STZ-treated rats was diminished by DLP (CSE inhibitor) co-administration (Fig. 2).

DCF kinetics (Fig. 3) and DHE fluorescence staining intensity (Fig. 4) showed that STZ-diabetic rats or DLP-treated nondiabetic rats exhibited higher ($P < 0.05$) ROS levels, compared to nondiabetic control group. NaHS or moxonidine reversed the increase in ROS level in STZ-diabetic rats (Figs. 3 and 4), and DLP diminished the favorable effect of moxonidine (6 mg/kg) on RVLM redox status in STZ-diabtic rats (Figs. 3 and 4). Further, NaHS attenuated the increased ROS level and neuronal damage in STZ-treated rats, but it had no effect in control rats (Figs. 1-4).

Moxonidine or NaHS restores CSE, HO-1 and TH in the RVLM of diabetic rats.

Western blot analysis showed increase ($P<0.05$) in TH (Fig. 5A), and reductions ($P<0.05$) in CSE (Fig, 5B) and HO-1 (Fig. 5C), expressions in the RVLM of STZ diabetic rats, compared to nondiabetic control rats. NaHS or moxonidine reversed these STZ-evoked effects and restored the protein levels of these enzymes to nondiabetic control levels (Fig. 5). Except for DLP-evoked reduction ($P<0.05$) in CSE, NaHS or DLP had no effect on the expression level of these proteins in the RVLM of nondiabetic control rats (Fig. 5). However, DLP co-administration prevented the restoration of RVLM CSE, HO-1 and TH levels caused by moxonidine (6 mg/kg) in STZ-diabetic rats (Fig. 5). Finally, CSE activity was substantially ($P<0.05$) reduced in the RVLM of STZ-diabetic rats and DLP-treated nondiabetic rats (Fig. 6). NaHS or moxonidine (6 mg/kg) reversed the reduction in CSE activity in the RVLM of STZ-diabetic rats, and concurrent DLP administration prevented the favorable effect of moxonidine on RVLM CSE activity (Fig. 6).

Discussion

The present study is the first to discern a physiological neuroprotective role for H_2S in a major cardiovascular regulating nucleus, the RVLM. Our findings also suggest H_2S-dependent neuroprotective effect for moxonidine (I_1 agonist) against the diabetes-induced RVLM neuronal injury, oxidative stress and sympathoexcitation. The main findings that support our conclusions are: (i) NaHS (H_2S donor) or moxonidine mitigated the diabetes-induced RVLM neuronal injury, apoptosis, and oxidative stress-linked sympathoexcitation. (ii) Either intervention reversed the diabetes-induced reductions in CSE activity and in CSE and HO-1 expressions in the RVLM. (iii) CSE inhibition (DLP) reproduced a diabetic RVLM phentotype in nondiabetic rats, and nullified the favorable RVLM neuroprotective effects of moxonidine. Together, these findings implicate CSE/H_2S in moxonidine-evoked alleviation of diabetes-evoked neurotoxicity.

Our recent study raised important questions about the mechanism of the sympathoexcitation, which was associated with hypertension and autonomic dysregulation in diabetic rats (El-Sayed et al., 2016). Here, we addressed this question by testing the hypothesis that RVLM oxidative stress/neurotoxicity plays a pivotal role in these diabetes-evoked effects for the following reasons. First, the impaired glycemic control, associated with diabetes, activates RVLM neurons (Oshima et al., 2017), although this evidence was obtained in vitro and the mechaisms of this effect remain unknown. Second, whether the inhibition of CSE-derived H_2S, which contributes to diabetes-evoked cardiac and autonomic dysfunction in vivo (El-Sayed et al., 2016), occurs and accounts for similar effects in the RVLM has not been investigated. To

address these questions, we conducted detailed studies on the RVLM tissues obtained from diabetic and control rats used in our recent study (El-Sayed et al., 2016).

As an important foundation, our current study showed that STZ diabetic rats exhibited RVLM injury as indicated by the number of degenerated neurons identified by fluorojade C staining (Fig. 1), and by increased neuronal apoptosis (Fig. 2). While this new finding replicates neurotoxicity in other brain nuclei of the same model (Wang et al., 2014), the mechanism of such neurotoxicity has not been investigated.

We focused on neuronal oxidative stress as an underlying mechanism for the diabetes-evoked neuronal injury and sympathoexcitation based on current evidence in different model systems (Wang et al., 2014; Fouda and Abdel-Rahman, 2017; Oshima et al., 2017). In accordance with current guidelines (Griendling et al., 2016), we confirmed the diabetes-evoked increase in RVLM ROS by two different assays (DCF and DHE). Evidence suggests that the diabetes-evoked neuronal oxidative stress, observed here (Figs. 3 and 4) and in reported studies, could be caused by glucose autoxidation, endoplasmic reticulum stress and impaired antioxidant defenses (Li et al., 2005; Correia et al., 2008) as well as the increased vulnerability of the brain to oxidative stress (Carvalho et al., 2012; Duarte et al., 2013).

Results of the present study and reported findings suggest a causal role for local oxidative stress in the diabetes-evoked sympathoexcitation (increased TH, Fig. 5A) in the RVLM. Notably, TH in the RVLM reflects sympathetic activity (Guyenet, 2006) and oxidative stress induces sympathoexcitation in brain stem nuclei (Zimmerman and Davisson, 2004; Huang et al., 2006; Fujita et al., 2012). Further, sympathoexcitation exacerbates neurodegeneration (Burke et al., 2004), and may contribute to

cardiovascular anomalies in the same STZ-diabetic rats (El-Sayed et al., 2016) because the RVLM serves a pivotal role in blood pressure regulation (Pilowsky and Goodchild, 2002; Madden and Sved, 2003).

The present finddings suggest a pivotal role for CSE/H_2S downregulation (Fig. 5B) in diabetes-induced oxidative stress and the subsequent RVLM neurotoxicity (Figs. 1-5) given the anti-oxidant and anti-inflammatory actions of H_2S (Mustafa et al., 2009). This premise is supported by the ability of CSE inhibition (DLP) to cause oxidative stress and to reproduce the diabetic phenotype in the RVLM of non-diabetic rats. Notably, the new finding that DLP reduced CSE protein levels in these non-diabetic rats (Fig. 5B) likely resulted from DLP-evoked oxidative stress (Figs. 3 and 4) via the inhibition of CSE catalytic activity (Fig. 6). This possibility is supported by the finding that H_2O_2-evoked oxidative stress suppressed CSE protein level in cultured cells (Manna et al., 2014), and by the inverse relationship between ROS and CSE expression in the RVLM (Figs. 3-5), and liver (Manna et al., 2014), of STZ-diabetic rats. These findings suggest an inhibitory role for oxidative stress on CSE protein expression, and identify CSE/H_2S upregulation as a novel target for the alleviatation of RVLM neurotoxicity in diabetes.

Results of the present study show that moxonidine inhibits sympathoexcitaion (Fig. 5A) and neuronal death (Figs. 1 and 2) in diabetic rats. These findings agree with neuroprotective effects of moxonidine against ischemic insults in neuronal cultures (Milhaud et al., 2000; Bakuridze et al., 2009) and against glutamate-evoked neurotoxicity (Keller and Garcia-Sevilla, 2016). However, the mechanism of the neuroprotective effect of moxonidine was not investigated in the reported studies.

JPET Fast Forward. Published on November 13, 2017 as DOI: 10.1124/jpet.117.243865
This article has not been copyedited and formatted. The final version may differ from this version.

Our findings suggest a pivotal role for RVLM CSE/H_2S upregulation in moxonidine-evoked neuroprotection and sympathoinhibition because these responses were tightly correlated in moxonidine-treated diabetic rats and were abolished in the presence of CSE inhibition (DLP). These findings are consistent with neuroprotective effect of H_2S and its anti-apoptotic effect through increasing glutathione level and suppressing oxidative stress (Kimura and Kimura, 2004; Kimura et al., 2010; Mikami et al., 2016). These reported findings raised the possibility that H_2S interacts with another antioxidant gaseous neuromodulator, HO-1.

We studied the role of HO-1 in our model system because it is expressed in the RVLM neurons (Mazza et al., 2001), exerts neuronal anti-oxidant and anti-apoptotic effect (Spitz et al., 1987; Fouda and Abdel-Rahman, 2017; Kim et al., 2017), and mediates sympathoinhibition (Nassar et al., 2011). Our findings suggest H_2S-dependent regulation of HO-1 in the RVLM contributes to the diabetes-evoked neurotoxicity and its alleviation by moxonidine for the following reasons. First, CSE/H_2S inhibition in diabetic rats, and in healthy rats following DLP, was associated with reduced RVLM HO-1 expression (Fig. 5C). Second, the H_2S donor NaHS or moxonidine restored RVLM HO-1 expression in diabetic rats (Fig. 5C). Third, CSE inhibition (DLP) abolished the moxonidine-evoked restoration of HO-1 expression in diabetic rats (Fig. 5C).

The present findings provide two new pieces of evidence. First, CSE/H_2S inhibition mediates neuronal injury, oxidative stress and increased pre-sympathetic neuronal activity in the RVLM in diabetic rats. Second, restoration of RVLM CSE-derived H_2S mediates the sympathoinhibitory and neuroprotective actions of moxonidine in diabetes. The neuropathological consequences of diabetes and their reversal by moxonidine might

JPET Fast Forward. Published on November 13, 2017 as DOI: 10.1124/jpet.117.243865
This article has not been copyedited and formatted. The final version may differ from this version.

explain the cardiovascular anomalies and their alleviation by moxonidine, respectively, in our previous in vivo study (El-Sayed et al., 2016). The findings also suggest that H_2S confers neuroprotection and sympathoinhibition, at least partly, via HO-1, and highlight the RVLM CSE/HO-1 pathway as a viable target for developing novel therapeutics for alleviating the neurotoxicity and cardiovascular anomalies associated with diabetes.

Acknowledgements

The authors thank Kui Sun and Dr. Fanrong Yao for technical assistance.

Authorship contributions

Participated in research design: Fouda, El-Sayed and Abdel-Rahman.

Conducted experiments: Fouda.

Performed data analysis: Fouda.

Contributed to writing of the manuscript: Fouda and Abdel-Rahman.

Reference:

Abdel Moneim AE (2015) The neuroprotective effect of berberine in mercury-induced neurotoxicity in rats. *Metab Brain Dis* **30**:935-942.

Bahniwal M, Little JP and Klegeris A (2017) High Glucose Enhances Neurotoxicity and Inflammatory Cytokine Secretion by Stimulated Human Astrocytes. *Curr Alzheimer Res*.

Bakuridze K, Savli E, Gongadze N, Bas DB and Gepdiremen A (2009) Protection in glutamate-induced neurotoxicity by imidazoline receptor agonist moxonidine. *Int J Neurosci* **119**:1705-1717.

Biessels GJ, van der Heide LP, Kamal A, Bleys RL and Gispen WH (2002) Ageing and diabetes: implications for brain function. *Eur J Pharmacol* **441**:1-14.

Burke WJ, Li SW, Chung HD, Ruggiero DA, Kristal BS, Johnson EM, Lampe P, Kumar VB, Franko M, Williams EA and Zahm DS (2004) Neurotoxicity of MAO metabolites of catecholamine neurotransmitters: role in neurodegenerative diseases. *Neurotoxicology* **25**:101-115.

Carvalho C, Cardoso S, Correia SC, Santos RX, Santos MS, Baldeiras I, Oliveira CR and Moreira PI (2012) Metabolic alterations induced by sucrose intake and Alzheimer's disease promote similar brain mitochondrial abnormalities. *Diabetes* **61**:1234-1242.

Ceretta LB, Reus GZ, Abelaira HM, Ribeiro KF, Zappellini G, Felisbino FF, Steckert AV, Dal-Pizzol F and Quevedo J (2012) Increased oxidative stress and imbalance in antioxidant enzymes in the brains of alloxan-induced diabetic rats. *Exp Diabetes Res* **2012**:302682.

Chaparro RE, Quiroga C, Bosco G, Erasso D, Rubini A, Mangar D, Parmagnani A and Camporesi EM (2013) Hippocampal cellular loss after brief hypotension. *Springerplus* **2**:23.

Collin B, Busseuil D, Zeller M, Perrin C, Barthez O, Duvillard L, Vergely C, Bardou M, Dumas M, Cottin Y and Rochette L (2007) Increased superoxide anion production is associated with early atherosclerosis and cardiovascular dysfunctions in a rabbit model. *Mol Cell Biochem* **294**:225-235.

Correia S, Carvalho C, Santos MS, Seica R, Oliveira CR and Moreira PI (2008) Mechanisms of action of metformin in type 2 diabetes and associated complications: an overview. *Mini Rev Med Chem* **8**:1343-1354.

Diwakar L and Ravindranath V (2007) Inhibition of cystathionine-gamma-lyase leads to loss of glutathione and aggravation of mitochondrial dysfunction mediated by excitatory amino acid in the CNS. *Neurochemistry international* **50**:418-426.

Duarte AI, Candeias E, Correia SC, Santos RX, Carvalho C, Cardoso S, Placido A, Santos MS, Oliveira CR and Moreira PI (2013) Crosstalk between diabetes and brain: glucagon-like peptide-1 mimetics as a promising therapy against neurodegeneration. *Biochim Biophys Acta* **1832**:527-541.

El-Sayed SS, Zakaria MN, Abdel-Ghany RH and Abdel-Rahman AA (2016) Cystathionine-gamma lyase-derived hydrogen sulfide mediates the cardiovascular protective effects of moxonidine in diabetic rats. *Eur J Pharmacol* **783**:73-84.

Fouda MA and Abdel-Rahman AA (2017) Endothelin Confers Protection against High Glucose-Induced Neurotoxicity via Alleviation of Oxidative Stress. *The Journal of pharmacology and experimental therapeutics* **361**:130-139.

Fujita M, Ando K, Kawarazaki H, Kawarasaki C, Muraoka K, Ohtsu H, Shimizu H and Fujita T (2012) Sympathoexcitation by brain oxidative stress mediates arterial pressure elevation in salt-induced chronic kidney disease. *Hypertension* **59**:105-112.

Giacco F and Brownlee M (2010) Oxidative stress and diabetic complications. *Circ Res* **107**:1058-1070.

Griendling KK, Touyz RM, Zweier JL, Dikalov S, Chilian W, Chen YR, Harrison DG, Bhatnagar A and American Heart Association Council on Basic Cardiovascular S (2016) Measurement of Reactive Oxygen Species, Reactive Nitrogen Species, and Redox-Dependent Signaling in the Cardiovascular System: A Scientific Statement From the American Heart Association. *Circulation research* **119**:e39-75.

Guo Q, Jin S, Wang XL, Wang R, Xiao L, He RR and Wu YM (2011) Hydrogen sulfide in the rostral ventrolateral medulla inhibits sympathetic vasomotor tone through ATP-sensitive K+ channels. *J Pharmacol Exp Ther* **338**:458-465.

Guyenet PG (2006) The sympathetic control of blood pressure. *Nat Rev Neurosci* **7**:335-346.

Huang BS, Amin MS and Leenen FH (2006) The central role of the brain in salt-sensitive hypertension. *Curr Opin Cardiol* **21**:295-304.

Ibrahim BM and Abdel-Rahman AA (2015) A pivotal role for enhanced brainstem Orexin receptor 1 signaling in the central cannabinoid receptor 1-mediated pressor response in conscious rats. *Brain Res* **1622**:51-63.

Keller B and Garcia-Sevilla JA (2016) Inhibitory effects of imidazoline receptor ligands on basal and kainic acid-induced neurotoxic signalling in mice. *J Psychopharmacol* **30**:875-886.

Kim S, Chin YW and Cho J (2017) Protection of Cultured Cortical Neurons by Luteolin against Oxidative Damage through Inhibition of Apoptosis and Induction of Heme Oxygenase-1. *Biol Pharm Bull* **40**:256-265.

Kimura Y, Goto Y and Kimura H (2010) Hydrogen sulfide increases glutathione production and suppresses oxidative stress in mitochondria. *Antioxid Redox Signal* **12**:1-13.

Kimura Y and Kimura H (2004) Hydrogen sulfide protects neurons from oxidative stress. *FASEB J* **18**:1165-1167.

Konno S, Hirooka Y, Kishi T and Sunagawa K (2012) Sympathoinhibitory effects of telmisartan through the reduction of oxidative stress in the rostral ventrolateral medulla of obesity-induced hypertensive rats. *J Hypertens* **30**:1992-1999.

Li ZG, Zhang W and Sima AA (2005) The role of impaired insulin/IGF action in primary diabetic encephalopathy. *Brain Res* **1037**:12-24.

Madden CJ and Sved AF (2003) Rostral ventrolateral medulla C1 neurons and cardiovascular regulation. *Cell Mol Neurobiol* **23**:739-749.

Manna P, Gungor N, McVie R and Jain SK (2014) Decreased cystathionine-gamma-lyase (CSE) activity in livers of type 1 diabetic rats and peripheral blood

mononuclear cells (PBMC) of type 1 diabetic patients. *The Journal of biological chemistry* **289**:11767-11778.

Marcus DL, Strafaci JA, Miller DC, Masia S, Thomas CG, Rosman J, Hussain S and Freedman ML (1998) Quantitative neuronal c-fos and c-jun expression in Alzheimer's disease. *Neurobiol Aging* **19**:393-400.

Mazza E, Thakkar-Varia S, Tozzi CA and Neubauer JA (2001) Expression of heme oxygenase in the oxygen-sensing regions of the rostral ventrolateral medulla. *J Appl Physiol (1985)* **91**:379-385.

Mikami Y, Kakizawa S and Yamazawa T (2016) Essential Roles of Natural Products and Gaseous Mediators on Neuronal Cell Death or Survival. *Int J Mol Sci* **17**.

Milhaud D, Fagni L, Bockaert J and Lafon-Cazal M (2000) Imidazoline-induced neuroprotective effects result from blockade of NMDA receptor channels in neuronal cultures. *Neuropharmacology* **39**:2244-2254.

Mukaddam-Daher S, Menaouar A, Paquette PA, Jankowski M, Gutkowska J, Gillis MA, Shi YF, Calderone A and Tardif JC (2009) Hemodynamic and cardiac effects of chronic eprosartan and moxonidine therapy in stroke-prone spontaneously hypertensive rats. *Hypertension* **53**:775-781.

Mustafa AK, Gadalla MM and Snyder SH (2009) Signaling by gasotransmitters. *Sci Signal* **2**:re2.

Nassar NN, Abdelsalam RM, Abdel-Rahman AA and Abdallah DM (2012) Possible involvement of oxidative stress and inflammatory mediators in the protective effects of the early preconditioning window against transient global ischemia in rats. *Neurochem Res* **37**:614-621.

Nassar NN, Li G, Strat AL and Abdel-Rahman AA (2011) Enhanced hemeoxygenase activity in the rostral ventrolateral medulla mediates exaggerated hemin-evoked hypotension in the spontaneously hypertensive rat. *The Journal of pharmacology and experimental therapeutics* **339**:267-274.

Oh GS, Pae HO, Lee BS, Kim BN, Kim JM, Kim HR, Jeon SB, Jeon WK, Chae HJ and Chung HT (2006) Hydrogen sulfide inhibits nitric oxide production and nuclear factor-kappaB via heme oxygenase-1 expression in RAW264.7 macrophages stimulated with lipopolysaccharide. *Free Radic Biol Med* **41**:106-119.

Oshima N, Onimaru H, Matsubara H, Uchida T, Watanabe A, Imakiire T, Nishida Y and Kumagai H (2017) Direct effects of glucose, insulin, GLP-1, and GIP on bulbospinal neurons in the rostral ventrolateral medulla in neonatal wistar rats. *Neuroscience* **344**:74-88.

Pilowsky PM and Goodchild AK (2002) Baroreceptor reflex pathways and neurotransmitters: 10 years on. *J Hypertens* **20**:1675-1688.

Rezq S and Abdel-Rahman AA (2016) Rostral Ventrolateral Medulla EP3 Receptor Mediates the Sympathoexcitatory and Pressor Effects of Prostaglandin E2 in Conscious Rats. *The Journal of pharmacology and experimental therapeutics* **359**:290-299.

Ruginsk SG, Mecawi AS, da Silva MP, Reis WL, Coletti R, de Lima JB, Elias LL and Antunes-Rodrigues J (2015) Gaseous modulators in the control of the hypothalamic neurohypophyseal system. *Physiology (Bethesda)* **30**:127-138.

Spitz DR, Dewey WC and Li GC (1987) Hydrogen peroxide or heat shock induces resistance to hydrogen peroxide in Chinese hamster fibroblasts. *J Cell Physiol* **131**:364-373.

Szczepanska-Sadowska E, Cudnoch-Jedrzejewska A, Ufnal M and Zera T (2010) Brain and cardiovascular diseases: common neurogenic background of cardiovascular, metabolic and inflammatory diseases. *J Physiol Pharmacol* **61**:509-521.

van den Born JC, Hammes HP, Greffrath W, van Goor H, Hillebrands JL and Complications DGIRTGDM (2016) Gasotransmitters in Vascular Complications of Diabetes. *Diabetes* **65**:331-345.

Velasco-Xolalpa ME, Barragan-Iglesias P, Roa-Coria JE, Godinez-Chaparro B, Flores-Murrieta FJ, Torres-Lopez JE, Araiza-Saldana CI, Navarrete A and Rocha-Gonzalez HI (2013) Role of hydrogen sulfide in the pain processing of non-diabetic and diabetic rats. *Neuroscience* **250**:786-797.

Wang JQ, Yin J, Song YF, Zhang L, Ren YX, Wang DG, Gao LP and Jing YH (2014) Brain aging and AD-like pathology in streptozotocin-induced diabetic rats. *J Diabetes Res* **2014**:796840.

Wang X and Abdel-Rahman AA (2002) Estrogen modulation of eNOS activity and its association with caveolin-3 and calmodulin in rat hearts. *American journal of physiology Heart and circulatory physiology* **282**:H2309-2315.

Wang X and Abdel-Rahman AA (2005) Effect of chronic ethanol administration on hepatic eNOS activity and its association with caveolin-1 and calmodulin in female rats. *Am J Physiol Gastrointest Liver Physiol* **289**:G579-585.

Yan YH, C CKC, Wang JS, Tung CL, Li YR, Lo K and Cheng TJ (2014) Subchronic effects of inhaled ambient particulate matter on glucose homeostasis and target organ damage in a type 1 diabetic rat model. *Toxicol Appl Pharmacol* **281**:211-220.

Yang LY, Chu YH, Tweedie D, Yu QS, Pick CG, Hoffer BJ, Greig NH and Wang JY (2015) Post-trauma administration of the pifithrin-alpha oxygen analog improves histological and functional outcomes after experimental traumatic brain injury. *Experimental neurology* **269**:56-66.

Zimmerman MC and Davisson RL (2004) Redox signaling in central neural regulation of cardiovascular function. *Prog Biophys Mol Biol* **84**:125-149.

Footnotes:

Dr. Mohamed Fouda is a visiting scholar from the Department of Pharmacology and Toxicology, Faculty of Pharmacy, Alexandria University, Egypt.

Shaimaa S. El-Sayed, current address is Zagazig University Faculty of Pharmacy.

Funding: This work was supported by the National Institutes of Health [2R01 AA14441-10].

Figure legends

Fig.1. FluoroJade C (FJC) positive cells examined in the RVLM of rats showing neurodegeneration. Representative images of FJC-positive cells in male rats treated with STZ (55 mg/kg, i.p. for 4 weeks) or its vehicle (buffer) receiving NaHS (H_2S donor, 3.4 mg/kg/day, i.p for 3 weeks after diabetes induction), DLP (CSE inhibitor,37.5 mg/kg, I.p. for 3 weeks after diabetes induction), moxonidine (2 or 6 mg/kg/day for 3 weeks after diabetes induction, gavage), combination of moxonidine and DLP or their vehicle (for 3 weeks after diabetes induction). (**J**) Group data showing the neurodegeneration expressed as the mean number of FJC positive cells measured using NIH ImageJ analysis of confocal images. Values are expressed as means ± SEM (n=5 rats/group). *P < 0.05 versus corresponding "Ctrl/veh" values; $^{\#}$P < 0.05 versus corresponding "STZ/veh" values. $^{\$}$P < 0.05 versus "STZ/MOX-6" values.

Fig.2. Immunohistochemical detection of caspase-3 examined in the RVLM of rats. Representative images of caspase-3 expression in male rats treated with STZ (55 mg/kg, i.p. for 4 weeks) or its vehicle (buffer) receiving NaHS (H_2S donor for three weeks after diabetes induction; 3.4 mg/kg/day), DLP (CSE inhibitor, 37.5 mg/kg, I.p. for 3 weeks after diabetes induction), moxonidine (2 or 6 mg/kg/day for 3 weeks after diabetes induction, gavage), combination of moxonidine and DLP or their vehicle (for 3 weeks after diabetes induction). (**J**) Group data showing the mean number of caspase-3 expression measured using NIH ImageJ analysis of confocal images. Values are expressed as means ± SEM (n=5 rats/group). *P < 0.05 versus corresponding "Ctrl/veh" values; $^{\#}$P < 0.05 versus corresponding "STZ/veh" values. $^{\$}$P < 0.05 versus "STZ/MOX-6" values.

Fig. 3. The 2′,7′-dichlorofluorescein biochemical assay of the generation of ROS showing the slopes (regression coefficients) of the regression lines representing the rate of ROS production in in the RVLM of male rats treated with STZ (55 mg/kg, i.p. for 4 weeks) or its vehicle (buffer) receiving NaHS (H_2S donor for three weeks after diabetes induction; 3.4 mg/kg/day), DLP (CSE inhibitor, 37.5 mg/kg, I.p. for 3 weeks after diabetes induction), moxonidine (2 or 6 mg/kg/day for 3 weeks after diabetes induction, gavage), combination of moxonidine and DLP or their vehicle (for 3 weeks after diabetes induction). Values are expressed as means ± SEM (n=5 rats/group). *P < 0.05 versus corresponding "Ctrl/veh" values; $^{\#}$P < 0.05 versus corresponding "STZ/veh" values. $^{\$}$P < 0.05 versus "STZ/MOX-6" values.

Fig. 4. Confocal images showing superoxide level indicated by dihydroethidium (DHE) staining (red) in the RVLM of male rats treated with STZ (55 mg/kg, i.p. for 4 weeks) or its vehicle (buffer) receiving NaHS (H_2S donor for three weeks after diabetes induction; 3.4 mg/kg/day), DLP (CSE inhibitor, 37.5 mg/kg, I.p. for 3 weeks after diabetes induction), moxonidine (2 or 6 mg/kg/day for 3 weeks after diabetes induction; gavage), combination of moxonidine and DLP or their vehicle (for 3 weeks after diabetes induction). Values are expressed as means ± SEM (n=5 rats/group). *P < 0.05 versus corresponding "Ctrl/veh" values; $^{\#}$P < 0.05 versus corresponding "STZ/veh" values. $^{\$}$P < 0.05 versus "STZ/MOX-6" values.

Fig. 5. Western blots analysis showing the protein expression in the RVLM of male rats treated with STZ (55 mg/kg, i.p. for 4 weeks) or its vehicle (buffer) receiving NaHS (H_2S donor for three weeks after diabetes induction; 3.4 mg/kg/day), DLP (CSE inhibitor; 37.5 mg/kg; I.p. for 3 weeks after diabetes induction), moxonidine (2 or 6 mg/kg/day for 3

weeks after diabetes induction, gavage), combination of moxonidine and DLP or their vehicle (for 3 weeks after diabetes induction). (**A**) TH ratio to GAPDH protein (housekeeping protein) and western bands depicting the protein expression are shown below the bar graphs. (**B**) CSE ratio to GAPDH protein (housekeeping protein) and western bands depicting the protein expression are shown below the bar graphs. (**C**) HO-1 ratio to β-actin protein (housekeeping protein) and western bands depicting the protein expression are shown below the bar graphs. Values are expressed as means ± SEM (n=5 rats/group). *P < 0.05 versus corresponding "Ctrl/veh" values; $^{\#}$P < 0.05 versus corresponding "STZ/veh" values. $^{\$}$P < 0.05 versus "STZ/MOX-6" values.

Fig. 6. H_2S synthesizing enzyme activity in the RVLM of male rats treated with STZ (55 mg/kg, i.p. for 4 weeks) or its vehicle (buffer) receiving NaHS (H_2S donor for three weeks after diabetes induction; 3.4 mg/kg/day), DLP (CSE inhibitor, 37.5 mg/kg; I.p. for 3 weeks after diabetes induction), moxonidine (2 or 6 mg/kg/day for 3 weeks after diabetes induction, gavage), combination of moxonidine and DLP or their vehicle (for 3 weeks after diabetes induction). Values are expressed as means ± SEM (n=5 rats/group). *P < 0.05 versus corresponding "Ctrl/veh" values; $^{\#}$P < 0.05 versus corresponding "STZ/veh" values. $^{\$}$P < 0.05 versus "STZ/MOX-6" values.

JPET Fast Forward. Published on November 13, 2017 as DOI: 10.1124/jpet.117.243865
This article has not been copyedited and formatted. The final version may differ from this version.

Figure 1

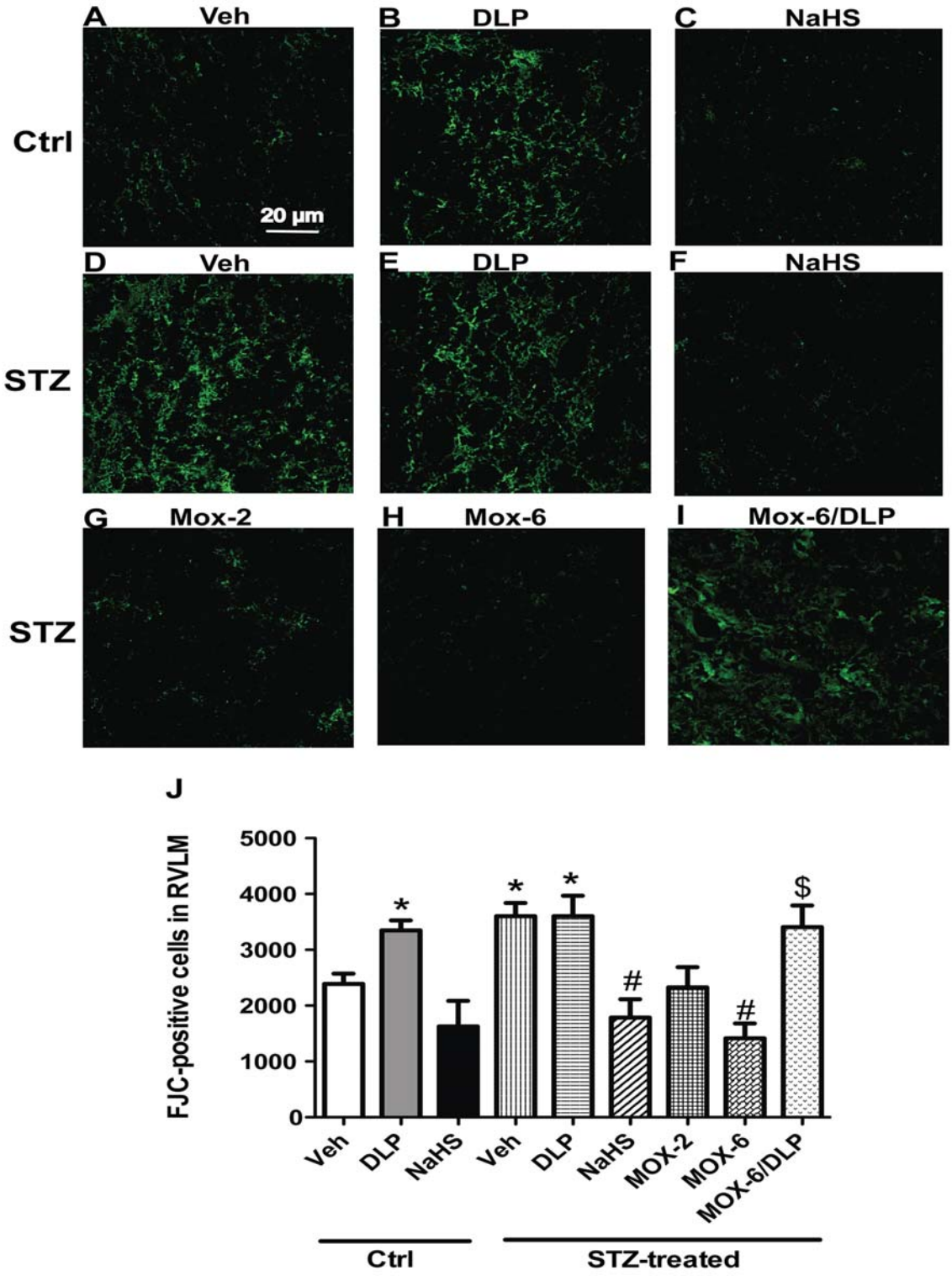

JPET Fast Forward. Published on November 13, 2017 as DOI: 10.1124/jpet.117.243865
This article has not been copyedited and formatted. The final version may differ from this version.

Figure 2

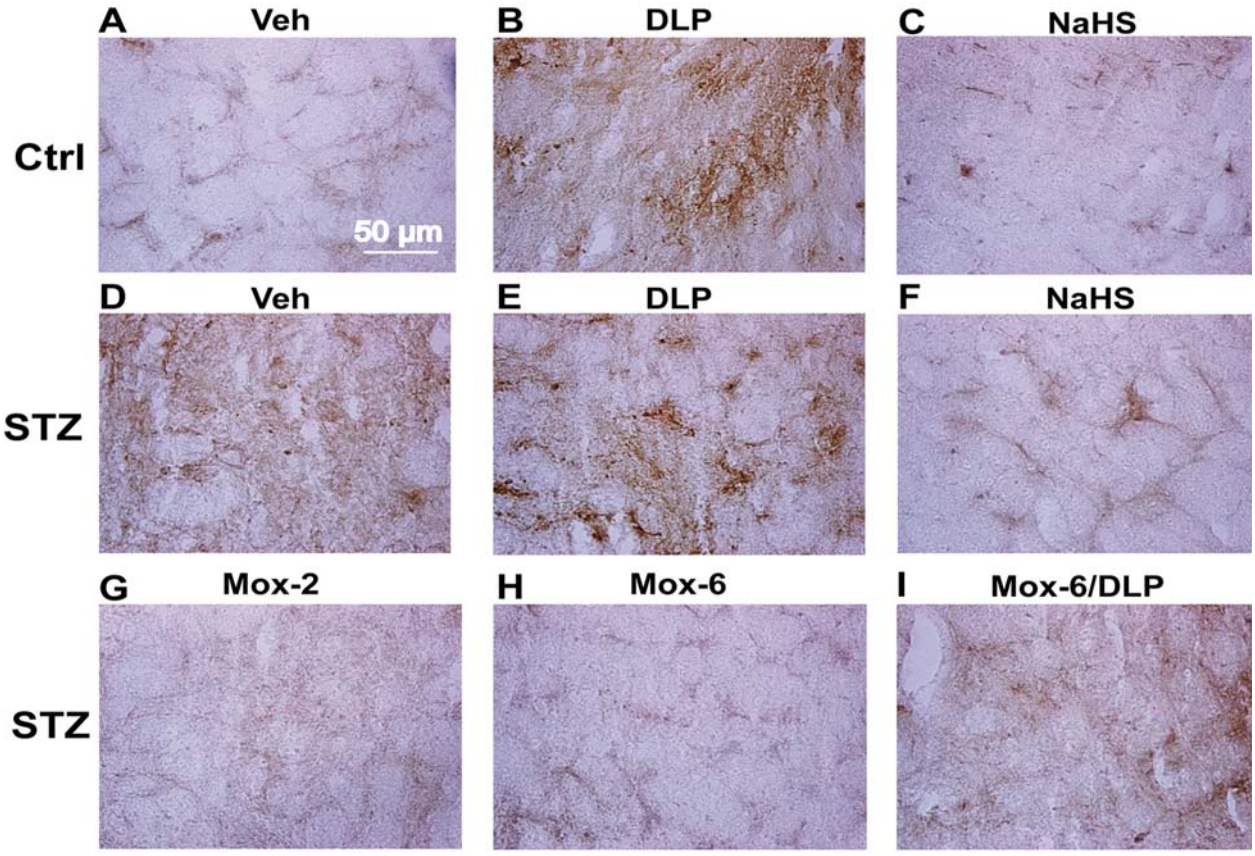

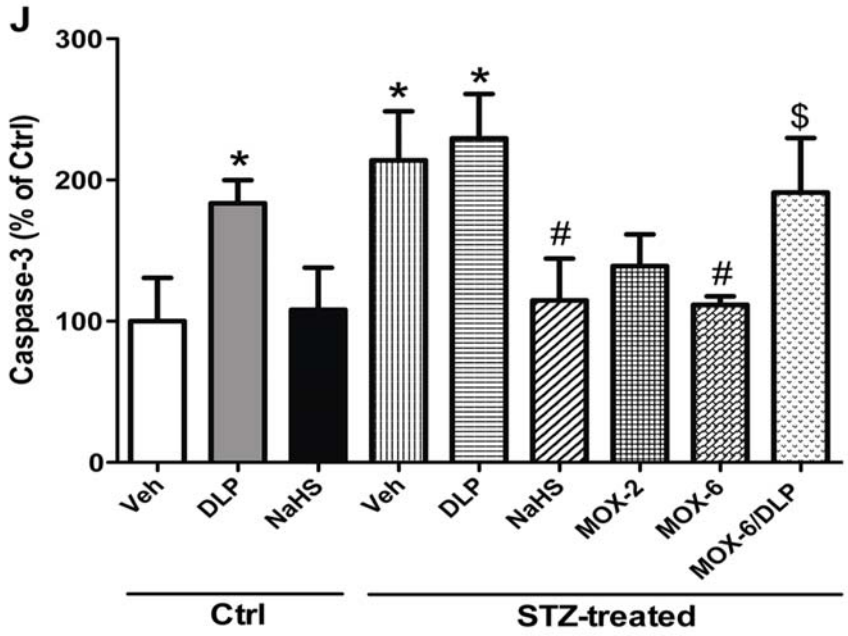

JPET Fast Forward. Published on November 13, 2017 as DOI: 10.1124/jpet.117.243865
This article has not been copyedited and formatted. The final version may differ from this version.

Figure 3

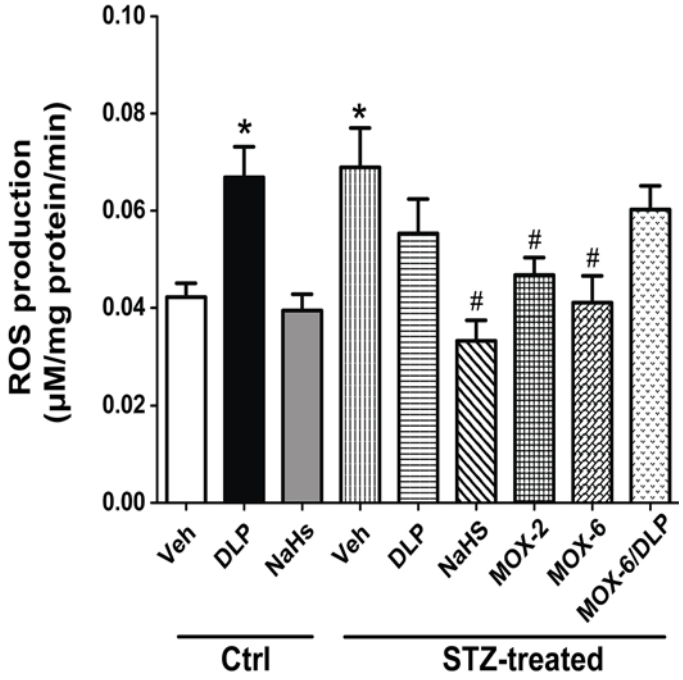

JPET Fast Forward. Published on November 13, 2017 as DOI: 10.1124/jpet.117.243865
This article has not been copyedited and formatted. The final version may differ from this version.

Figure 4

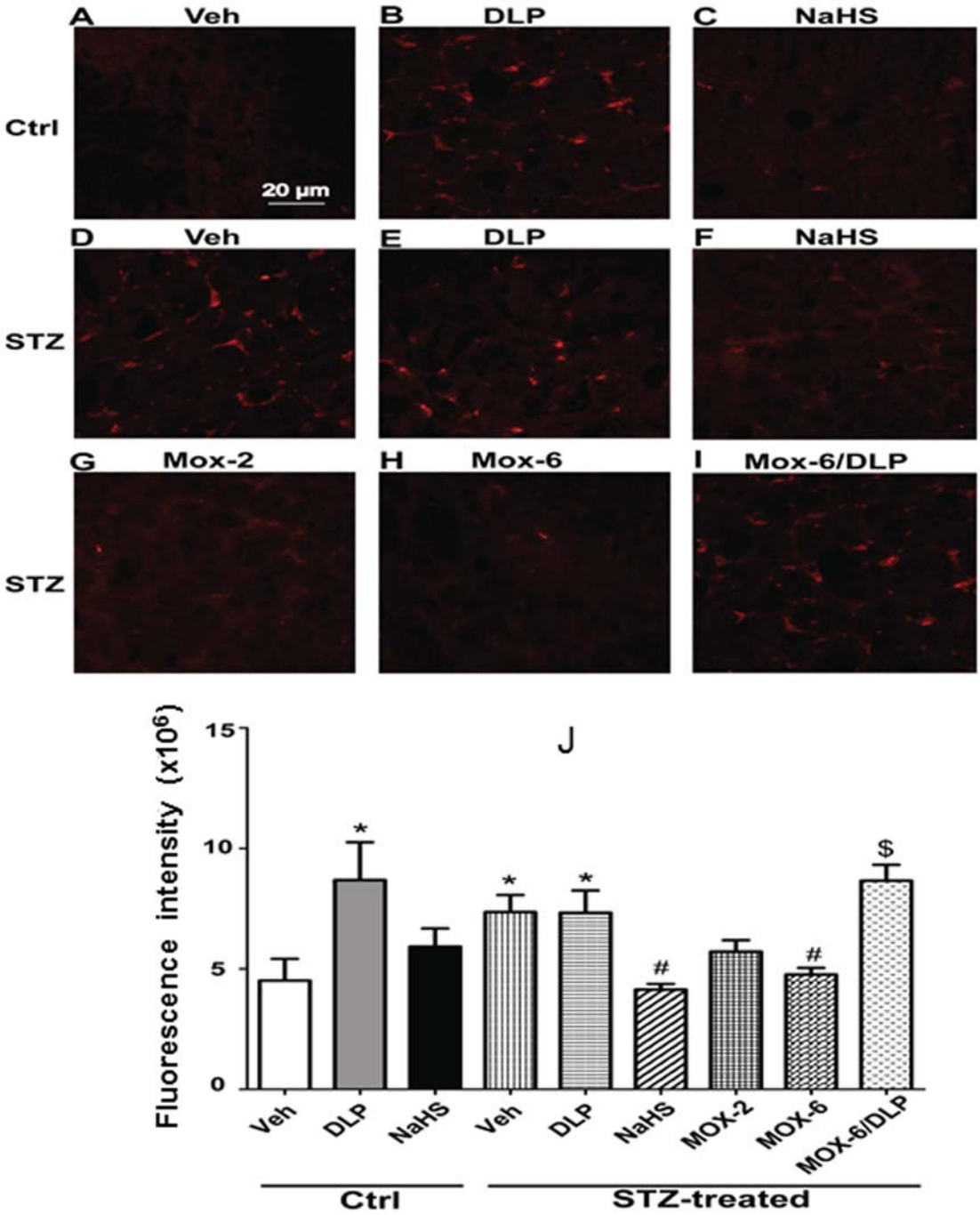

JPET Fast Forward. Published on November 13, 2017 as DOI: 10.1124/jpet.117.243865
This article has not been copyedited and formatted. The final version may differ from this version.

Figure 5

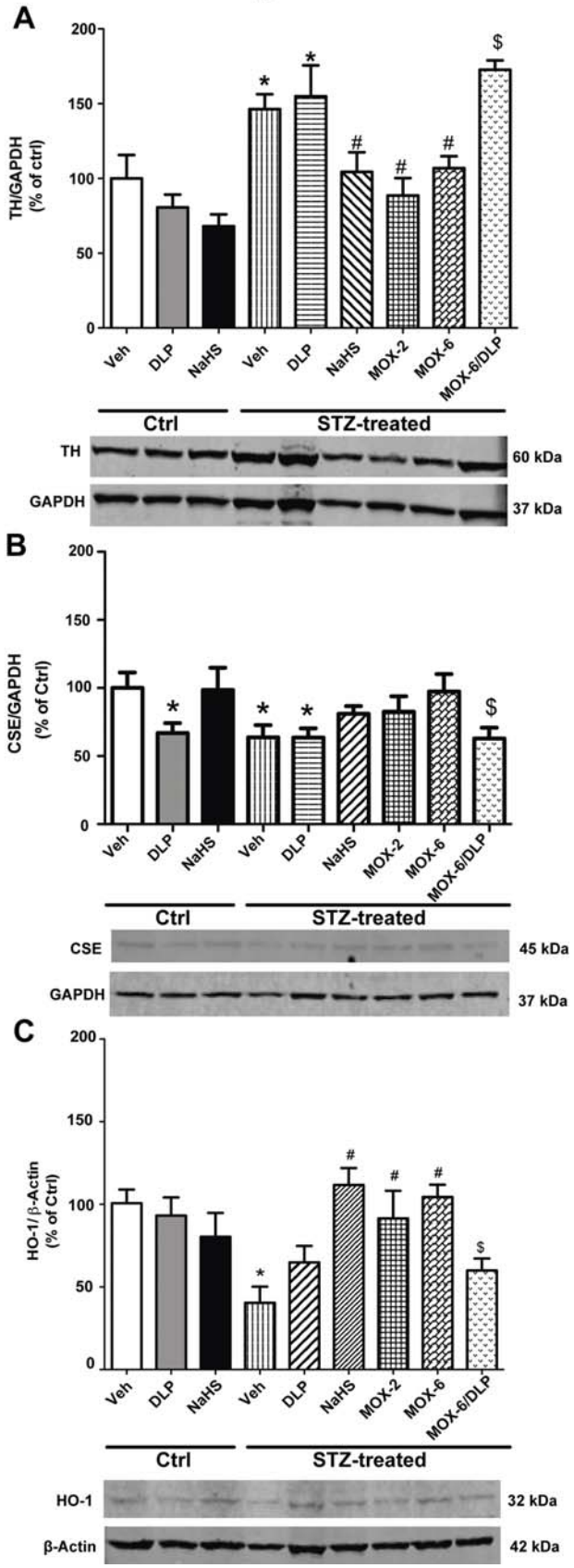

JPET Fast Forward. Published on November 13, 2017 as DOI: 10.1124/jpet.117.243865
This article has not been copyedited and formatted. The final version may differ from this version.

Figure 6